Heterogeneous distribution of inhibitory inputs among motor units as a key mechanism for motor adaptations to pain

François Hug[1,2]*, François Dernoncourt[1], Simon Avrillon[1], Jacob Thorstensen[2,3],
Manuela Besomi[4], Wolbert van den Hoorn[4,5], Kylie Tucker[2]

[1] Université Côte d'Azur, LAMHESS, Nice, France
[2] The University of Queensland, School of Biomedical Sciences, Brisbane, QLD, Australia
[3] Faculty of Health Sciences & Medicine, Bond University, Gold Coast, Australia
[4] The University of Queensland, Centre of Clinical Research Excellence in Spinal Pain, Injury and Health, School of Health and Rehabilitation Sciences, Brisbane, QLD, Australia
[5] School of Exercise and Nutrition Sciences, Queensland University of Technology, Brisbane, QLD, Australia

* Corresponding author
Prof. François Hug
Université Côte d'Azur, LAMHESS, Nice, France
Francois.hug@univ-cotedazur.fr

Running title: Inhibitory pattern of motor units during pain

Supplemental data availability: The entire dataset (raw and processed data) is available at: https://figshare.com/s/8b978f1cd32d8329266e; and the in-silico model is available at: https://github.com/FrancoisDernoncourt/Pain_inhibition_simulation

Conflict of interests: The authors declare no competing financial interests.

Funding resources: François Hug is supported by the French government, through the UCAJEDI Investments in the Future project managed by the National Research Agency (ANR) with the reference number ANR-15-IDEX-01 and by an ANR grant (ANR-24-CE17-5805, NEUROMOTOR project).

Author Contributions: Contribution and design of the experiment: FH, JT, MB, KT; Collection of data: FH, WvdH, KT; Analysis: FH, FD, SA; Drafting the article or revising it for important intellectual content: FH, FD, SA, JT, MB, WvdH, KT; All authors approved the final version of the manuscript.

Abstract.

Pain significantly influences movement, yet the precise neural mechanisms underlying the wide range of observed motor adaptations remain unclear. This study combined experimental data and *in silico* models to investigate the contribution of inhibitory and neuromodulatory inputs to motor unit behaviour during submaximal contractions performed in the presence of pain. Specifically, we aimed to unravel the distribution pattern of inhibitory inputs to the motor unit pool. Seventeen participants performed isometric knee extension tasks under three conditions: Control, Pain (induced by injecting hypertonic saline into the infra-patellar fat pad), and Washout. We identified large samples of motor units in the vastus lateralis (up to 53/participant) from high-density electromyographic signals, which led to three key observations. First, while motor unit discharge rates significantly decreased during Pain, a substantial proportion of motor units (14.8-24.8%) did not show this decrease and, in some cases, even exhibited an increase. Second, using complementary approaches we showed that pain did not alter the amplification and prolongation effects of persistent inward currents on motor unit discharge, providing evidence that neuromodulatory drive to motor neurons remained unchanged. Third, we observed a significant reduction in the proportion of common inputs to motor units during Pain. To explore potential neurophysiological mechanisms underlying these experimental results, we simulated the behaviour of motor unit pools with varying distribution patterns of inhibitory inputs. Our simulation supports the hypothesis of a non-homogeneous distribution of inhibitory inputs, independent of motor unit size, as a key neural mechanism underlying motor adaptations to experimental pain.

Keywords: motor neuron, persistent inward currents, principal component analysis, electromyography, common input.

Significance statement. Our study challenges the traditional view of homogeneous inhibition of motor units during noxious stimulation and strongly supports contemporary pain theories that propose a non-homogeneous distribution of inhibitory inputs across the motor unit pool. Although previous research has observed differential motor unit responses to pain - some with decreased discharge rates and others with increased discharge rates - these findings alone cannot distinguish between homogeneous and non-homogeneous inhibition. By combining experimental data with *in silico* modelling, we provide compelling evidence of increased inhibition that is non-uniformly distributed across motor units, independent of motor unit size, as a key neural mechanism underlying motor adaptations to pain.

1. Introduction

Pain affects movement, but the neural mechanisms underlying these motor adaptations are not well defined. As the final common pathway for movement control (1), spinal motor neurons transmit neural signals from various sources to muscle fibres. As such, measuring spinal motor neuron activity during nociceptive stimulation offers valuable insights into the motor adaptations to pain. In humans, this has been achieved by recording the spiking activity of single motor units (comprising a spinal motor neuron and the muscle fibres it innervates) in the presence of experimentally induced pain. Most studies report an overall reduction in motor unit discharge rates in muscles that are closely associated with the painful region (2-5). However, this overall (average) decrease in motor unit discharge rate is typically accompanied by an increase in the discharge rate of a small proportion of motor units and the recruitment of new units (4, 6-8). This multifaceted motor adaptation to pain is thought to assist with the maintenance of force output; however, the neural basis for these differential effects of nociceptive stimulation across the motor unit pool remains unknown.

The current literature does not clearly establish whether the differential effects of nociceptive stimulation arise from homogeneous or non-homogeneous patterns of inhibition. Martinez-Valdes et al. (8) observed that during submaximal contractions performed in the presence of pain, low-threshold motor units exhibited a decrease in discharge rate, while high-threshold units exhibited an increase. They proposed that this divergent effect arises from a non-homogeneous distribution of inhibitory afferent inputs, with greater inhibition directed toward low-threshold units; however, this has not yet been directly confirmed. It is important to note that these results are also compatible with a homogeneous distribution of inhibitory inputs, as such homogeneous inhibition would cause a greater inhibitory post-synaptic potential in low-threshold units (9). Either way, to compensate for inhibition and maintain force, increased excitatory input to the motoneuron pool may occur (10), potentially explaining the increased discharge rate of higher-threshold units (8). Notably, the divergent responses between low- and high threshold units could also involve differential changes in motor neuron intrinsic properties (11). For example, the reticular activating system, involved in the transmission and modulation of nociceptive information, releases monoamines (12), which may stimulate persistent inward currents. These currents amplify and extend the effects of synaptic input, and appear to have a greater influence on the discharge of low- than high-threshold units (13, 14). As persistent inward currents are sensitive to inhibition (15-17), homogeneous inhibition to the motor unit pool could have a greater impact on the persistent inward currents - and thus the discharge rate - of low-threshold units (11). In addition, there are observations that newly recruited higher-threshold units during pain do not always follow the expected orderly recruitment pattern (4). Combined with evidence of differential changes in motor neuron excitability within the pool (18), these deviations from the typical orderly recruitment pattern could suggest a non-homogeneous inhibition that is not strictly organised according to motor unit size.

Unravelling the distribution pattern of inhibition within the motor unit pool requires recording the activity of a large sample of motor units, which is not feasible using traditional methods that use a limited number of intramuscular electrodes (3, 4, 6). In this study, we identified a large sample of motor units (up to 53 per participant and contraction) by decomposing high-density electromyographic (EMG) signals. By combining experimental data and *in silico* models, we aimed to quantify the contribution of inhibitory and neuromodulatory inputs to the behaviour of motor unit populations during experimental joint pain.

2. Results

2.1. Experimental results

Seventeen participants performed a series of isometric submaximal knee extension tasks under three different conditions: Control, during the presence of experimental pain (Pain) and after pain had ceased (Washout). Pain was induced by injecting hypertonic saline into the infra-patellar fat pad. For each condition, participants performed one triangular force contraction (10-s ramp up and 10-s ramp down) to 30% of maximal voluntary contraction (MVC) and three trapezoidal force contractions (6-s ramp up followed by a 20-s plateau at 30% MVC) interspaced by 30-s of rest. EMG signals were recorded with four grids of 64 surface electrodes (a total of 256 electrodes) placed over the vastus lateralis (VL). A blind source-separation algorithm was applied to the EMG signals to identify motor units spike trains.

2.1.1. Pain

Participants reported an average pain intensity of 4.6±1.2 out of 10 before the trapezoidal contractions and 4.0±1.3 out of 10 before the triangular contractions. During contractions, the reported pain levels were 3.3±2.2 for the trapezoidal contractions and 4.0±1.6 for the triangular contractions. Pain was mainly localized around the injection site.

2.1.2. Force and interferential electromyography

Isometric force was measured using a three-dimensional force gauge (MC3A, AMTI, USA). Effective force (Fz), displayed as feedback and averaged across the three plateaus of the trapezoidal contractions, did not significantly differ between conditions (main effect of Condition: F(2,28)=3.0, p=0.066), as further supported by the very low coefficient of variation across conditions (1.2±0.9%). Similarly, the other force components did not change during Pain [Fx: F(2, 28)=0.8, p=0.47; Fy: F(2,28)=4.3, p=0.024 with post-hoc tests revealing no significant differences (all $p > 0.058$)].

The mean EMG amplitude calculated over the grid did not significantly differ between conditions [F(2,28)=0.91, p=0.42].

2.1.3. Motor unit yield

An average of 28.6±14.8 motor units (range: 7-53) and 22.3±11.3 motor units (range: 5-42) were identified per condition and participant during the trapezoidal and triangular contractions, respectively. We tracked motor units across the three conditions (Control, Pain, and Washout) for each task (trapezoidal and triangular contractions) separately. To achieve this, the separation vectors of the motor units identified in one condition were applied to the two other conditions (19). We successfully tracked 288 motor units for the trapezoidal contractions and 145 motor units for the triangular contractions. This resulted in an average of 19.2±13.3 (range: 5-41) motor units per participant for the trapezoidal contractions and 9.7±6.9 (range: 1-22) motor units per participant for the triangular contractions. All results presented below are based on these tracked motor units. The entire data set is available at https://figshare.com/s/8b978f1cd32d8329266e.

2.1.4. Motor unit discharge characteristics

2.1.4.1. Discharge rate

When considering the mean discharge rate across the three plateaus of the trapezoidal contractions, there was a main effect of condition (F(2, 856)=8.4, p<0.001; Figure 1). Specifically, the discharge rate was lower during Pain (8.9±1.6 pps) than both Control (9.3±1.7 pps; p = 0.02) and Washout (9.4±1.6 pps; p<0.001), with no difference between Control and Washout (p = 0.36). When considering the maximal discharge rate during the triangular contractions, there was also a main effect of condition (F(2, 430)=26.0, p< 0.001; Figure 1). Specifically, the discharge rate was significantly lower during Pain (11.1±1.7 pps) than both Control (12.2±1.8 pps; p <0.001) and Washout (12.3±1.7 pps; p < 0001), with no difference between Control and Washout (p=0.83).

Despite the significant decrease in motor unit discharge rate during Pain, a notable proportion of motor units did not exhibit such a decrease, i.e. 24.8% of motor units during trapezoidal contractions and 14.8% of motor units during triangular contractions (Figure 1). It is worth noting that when considering the group level, there was no significant correlation between the recruitment threshold measured during the Control condition and the change in discharge rate between Control and Pain, regardless of the task (trapezoidal: r=0.06; p=0.27; triangular: r=0.02; p=0.81; Figure 1). We also conducted this analysis for each individual participant and found no significant correlation in 11 out of 15 participants for the trapezoidal contractions (p-values ranging from 0.065 to 0.797) and in 11 out of 12 participants for the triangular contractions (p-values ranging from 0.140 to 0.934, with three participants excluded due to a low motor unit yield). Over the remaining participants who exhibited a significant correlation, one participant exhibited a negative correlation during both the trapezoidal (r=-0.52, p<0.001) and the triangular contractions (r=-0.72, p<0.001); and three participants exhibited a positive correlation (r ranging from 0.42 to 0.68; p-values ranging from 0.004 to 0.038).

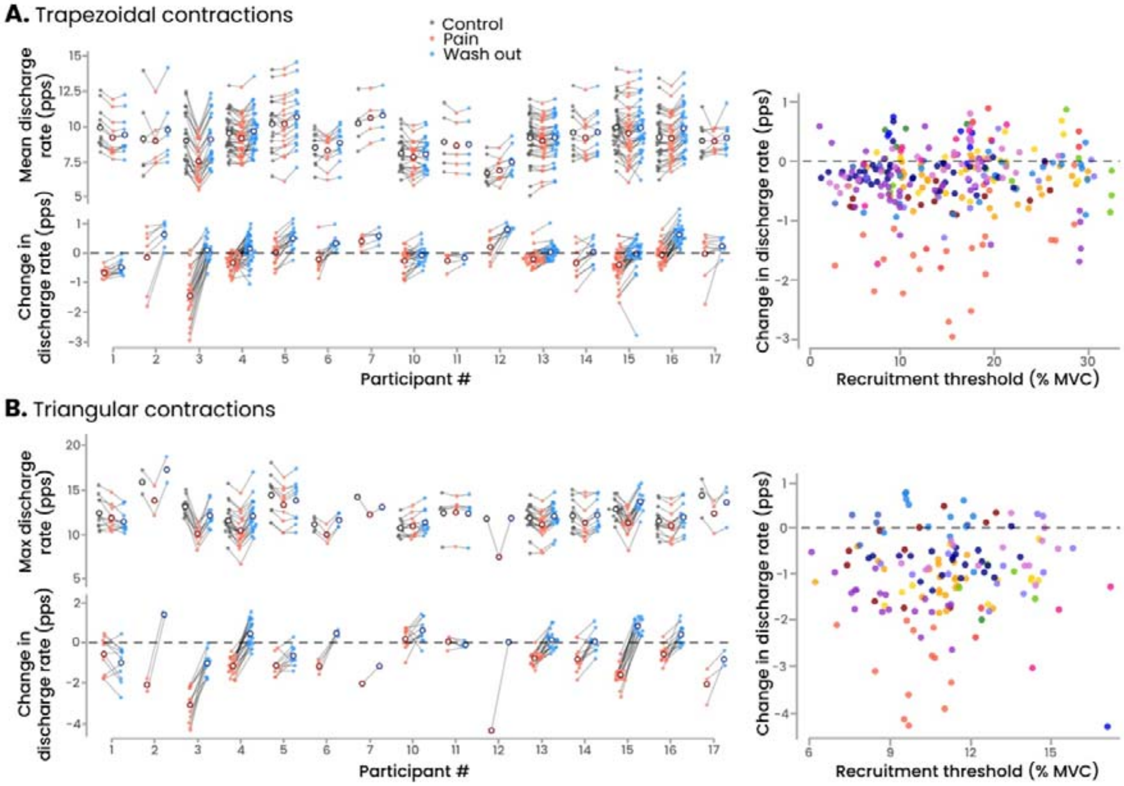

Figure 1. Change in discharge rate during pain. Panel A shows the discharge rate averaged over the plateau of the trapezoidal contractions for each participant (n=15) and condition (Control, Pain, and Washout). **Panel B** shows the maximal discharge rate measured during the triangular contraction for each participant (n=15) and condition. In both panels, the lower figure shows the change in discharge rate relative to the Control condition, and the right figure shows the relationship between the change in discharge rate during Pain and the recruitment threshold assessed during the Control condition. In left panels, each dot represents an individual motor unit and only motor units successfully tracked across all three conditions are included. The unfilled circles represent the mean values. In right panels each dot represents an individual motor unit and each colour represents a participant. Regardless of the task, there was a significant main effect of condition. The discharge rate was significantly lower during Pain compared to both Control and Washout, with no significant difference between Control and Washout. When considering the population level, there was no significant correlation between the change in discharge rate during Pain relative to Control and the recruitment threshold.

2.1.4.2. Estimates of neuromodulation

We estimated the magnitude of persistent inward currents using a paired motor unit analysis applied to the triangular contractions (20). Specifically, we assessed the discharge rate of a lower-threshold motor unit (control unit) at the time of recruitment and de-recruitment of a higher-threshold motor unit (test unit). The difference in instantaneous discharge rate between the recruitment and de-recruitment times of the test unit, referred to as ∆F, is considered proportional to the magnitude of persistent inward currents (20). Because we were unable to find any pairs of control/test units in three participants (including the two female participants), ΔF values are reported for 12 participants. There was a main effect of condition (F(2, 322) = 5.9, p = 0.003; Figure 2), with significantly lower ΔF values during Pain (2.2±1.3 pps) compared to Control (2.7±1.3 pps; p=0.002), corresponding to a decrease of 11.8±38.7% during Pain relative to Control. There was neither a difference between Pain and Washout (2.5±1.1 pps; p=0.11), nor between Control and Washout (p=0.32). Interestingly, there was a significant positive correlation between the change in maximal discharge rate between Control and Pain and the change in ΔF (r=0.61, p=0.035).

Because ΔF values depend on both neuromodulation and inhibition supplied to the pool of motor units (17, 21), we used complementary metrics to provide a more direct estimate of the neuromodulatory inputs. We quantified the deviation from a linear increase in discharge rate relative to actual torque during the ramp-up phase of the triangular contractions (brace height) and the rate of change in discharge (acceleration and attenuation) (21). Using this geometric approach, which enabled us to isolate the effects of neuromodulation from inhibition (21, 22), we found no main effect of Condition, regardless of the metric considered: acceleration (F(2, 430) = 2.2, p = 0.11), attenuation (F(2, 430) = 0.37, p = 0.69), and brace height (F(2, 430) = 1.91, p = 0.15) (Figure 2).

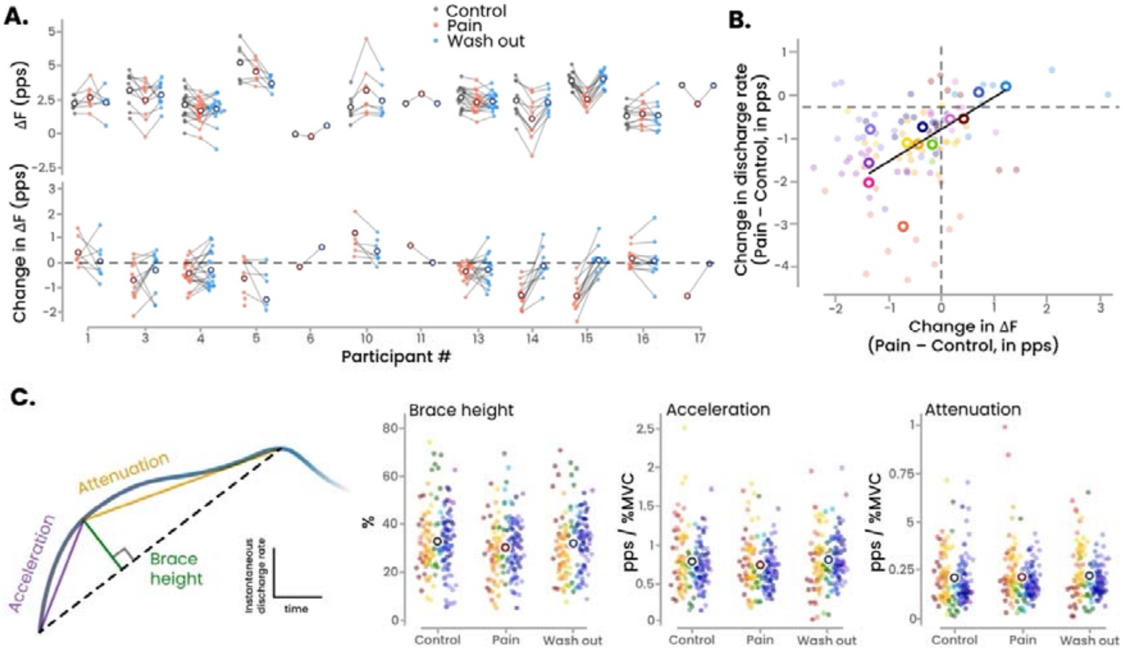

Figure 2. Neuromodulatory input. Panel A displays the ΔF values for each participant and condition (Control, Pain, and Washout), with the lower portion showing the change in ΔF during Pain relative to

Control (n=12). There was a main effect of Condition, with significant lower ΔF values during Pain compared to Control, with no other significant differences. Note the absence of data for three participants who were excluded due to a low motor unit yield. **Panel B** shows the significant positive correlation between the change in ΔF during Pain relative to Control and the change in maximal discharge rate measured during the triangular contraction. Each dot represents a motor unit, and each colour represents a participant, with the mean for each participant represented by an unfilled circle (n=12). **Panel C** depicts the geometric approach used to estimate the strength of neuromodulatory inputs. Results are presented on three distinct graphs where each dot represents a motor unit, and each colour represents a participant (n=15). The group mean is represented by an unfilled circle. There was no significant main effect of condition, regardless of the metrics.

2.1.5. Common synaptic input

We used two different approaches to estimate the common synaptic inputs received by the motor neuron pool during the trapezoidal contractions.

First, we estimated the proportion of common input relative to the total input received by the motor neuron pool (23). We calculated the coherence between two equally sized groups of motor units, with the number of motor units in each group varying from 1 to half of the total number of identified units. The proportion of common synaptic inputs was derived from the relationship between the average coherence values in the 0-5 Hz bandwidth and the number of motor units in each group (see Methods). Because less than eight motor units were identified in three participants, these analyses were performed on the remaining 12 participants. There was a main effect of Condition on the estimated proportion of common synaptic input (F(2, 22) = 4.8; p=0.019). Specifically, the proportion of common input was significantly lower during Pain than both Control (-12.6±12.7%; p=0.031) and Washout (-9.1±15.4%; p=0.040), with no significant difference between Control and Washout (p=0.99).

Second, we applied a principal component analysis to the smoothed discharge rates over the plateaus of the trapezoidal contractions and we quantified the variance explained by the first principal component (24). There was a significant main effect of Condition (F(2, 22) = 6.0; p=0.008), with the variance of the first component being lower during Pain compared to both Control (-11.8±14.2%; p=0.041) and Washout (-12.7±18.6%; p=0.009). No significant difference was observed between Control and Washout (p=0.77).

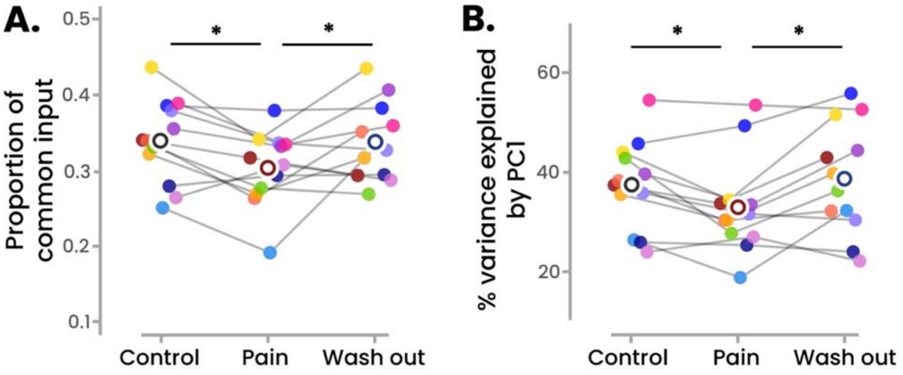

Figure 3. Estimates of common synaptic inputs. Two different approaches were used to estimate the common synaptic inputs received by the motor neuron pool during the trapezoidal contractions, i.e., the proportion of common synaptic input and the variance explained by the first principal component. Regardless of the metric, there was a main effect of condition, with significant lower values during Pain compared to Control. Asterisks indicate significant differences ($p<0.005$). Each dot represents a participant ($n=12$), and the unfilled circles represent the mean values. PC1, first principal component.

2.2. Simulation results

To explore potential neurophysiological mechanisms underlying the experimental results, we simulated the behaviour of a pool of 300 motor units with different distributions of inhibitory inputs. To this aim, we used a conductance-based leaky integrate-and-fire model where the simulated motor units received common excitatory input, common noise and independent noise. All the motor units within the pool received the same common excitatory input and common noise, while each motor unit received different independent noise. We tested six simulation scenarios. First, motor units received no inhibitory input (Control condition). Second, all motor units received a common inhibitory signal with the same weight (Homogeneous condition). Third, a common inhibitory signal was distributed to the motor unit pool following a decaying exponential function, with inhibition weights biased toward the low-threshold units (Gradient inhibition condition). A small standard deviation of 0.1 was added to account for slight variability in the weights. This condition was designed to test the hypothesis proposed by Martinez-Valdes et al. (8) of differential inhibitory input between low- and high-threshold motor units. Based on our results showing no systematic correlation between the change in discharge rate during pain and the recruitment threshold, the other scenarios were designed to test a heterogeneous distribution of inhibitory inputs to the motor unit pool. Specifically, a common inhibitory signal was assigned to motor units with random weights following a Gaussian distribution with either low (SD=0.2) or high (SD=0.5) variance (Heterogeneous inhibition conditions). In the final scenario, motor units were randomly divided into two groups. A common inhibitory signal was distributed to these groups, with a weight of 1.5 assigned to the first group, comprising 75% of the motor units, and a weight of 0.5 assigned to the second group, comprising 25% of the motor units (Clustered inhibition conditions). This ensured that the majority of motor units received a higher level of inhibition. The motivation for simulating clusters of inhibition stems from recent studies suggesting that motor units from the same pool may be grouped into different synergies based on the distinct net inputs they receive (25).

The mean level of inhibition was maintained constant across the five scenarios with inhibition, and the force was kept constant. Only one simulation was run for the Control condition, and ten simulations were run for the conditions with inhibition to account for slightly different distribution on inhibitory inputs across the simulations.

The main outcomes of the simulations are depicted in Figure 4. The six simulation scenarios produced realistic motor unit discharge rates, ranging from 10.4 pps under homogeneous inhibition to 13.0 pps in the Control scenario. Consistent with our experimental data, all simulation scenarios resulted in an overall decrease in discharge rates of the matched motor units, with a proportion of motor units exhibiting an increase in discharge rate to maintain force (ranging from 20.0±0.4% to 39.5±0.4% across all scenarios). In addition, some new motor units were recruited in the presence of inhibition, ranging from +1.7±1.0 (Clustered inhibition) to +6.7±0.7 (Gradient inhibition) motor units.

Compared to the Control scenario, the change in discharge rate across conditions varied from -1.4±0.0 pps for Gradient inhibition to -0.5±0.1 pps for Heterogeneous inhibition with high variance. When considering the estimates of common synaptic input, only three simulation scenarios aligned with our experimental data, showing a decrease in both the proportion of common input and the variance of the first principal component: the Gradient, Clustered, and Heterogeneous (high variance) distributions of inhibition (Figure 4). However, among these three scenarios, only two (Heterogeneous [high variance] and Clustered distribution) replicated the absence or weak relationship between the change in discharge rate and the recruitment threshold of the Control condition observed in our experimental data, with a mean $R^2<0.17$ (Figure 4). Notably, the Gradient distribution logically resulted in a very high R^2 value indicating a strong relationship between the change in discharge rate and the recruitment threshold. Overall, these simulation results demonstrate that only the two scenarios with high variability in the distribution of inhibitory inputs (Clustered and Heterogeneous [high variance] inhibition) successfully reproduced key features of our experimental data, i.e., an overall decrease in discharge rate regardless of motor unit size and a decrease in indexes of common synaptic input.

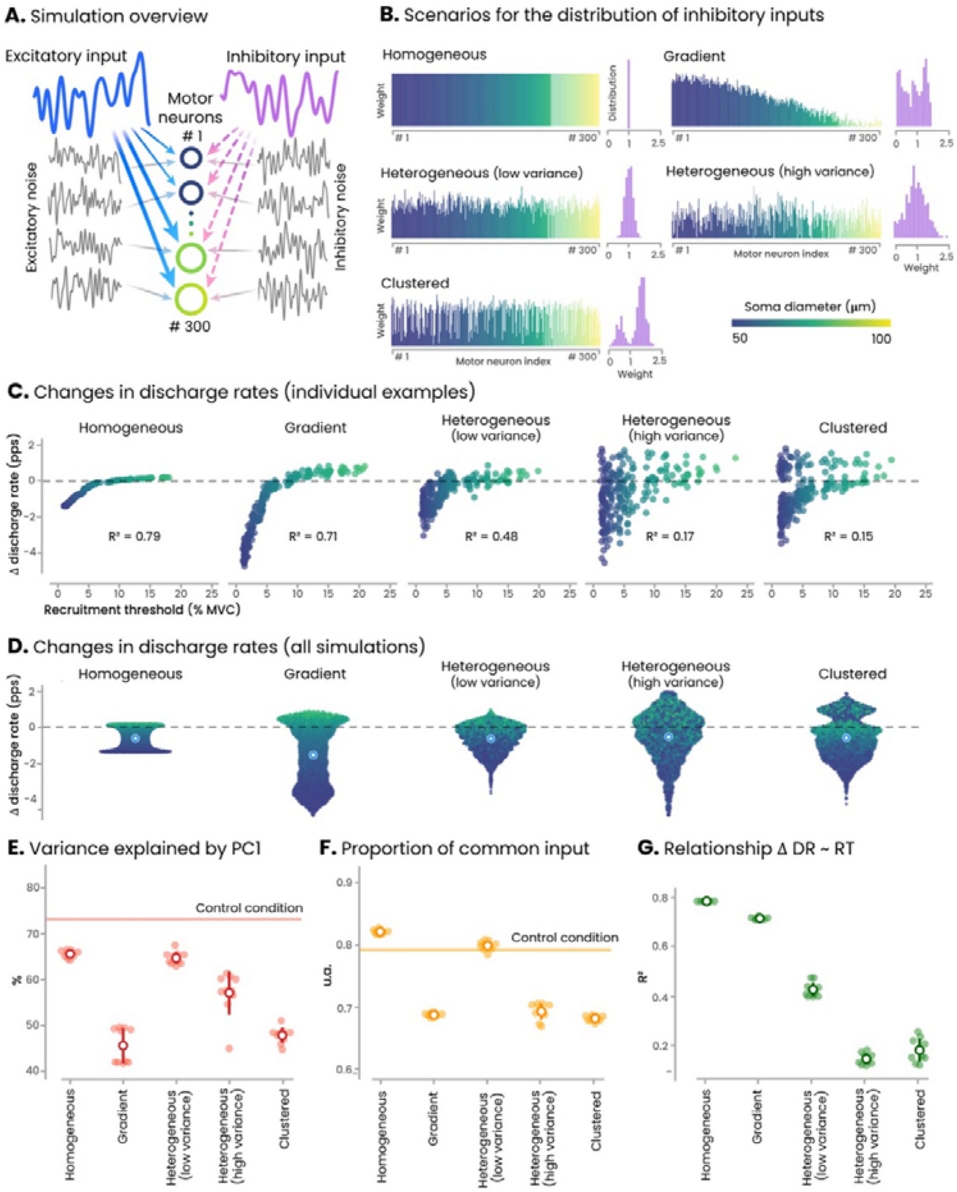

Figure 4. In-silico model. We simulated the behaviour of 300 motor unit using a conductance-based leaky integrate-and-fire model. **Panel A** illustrates the structure of the simulation model (see Methods for further details). **Panel B** presents the five simulated scenarios, distinguished by different distributions of inhibitory inputs. The weights of the inhibitory input were distributed as follows: 1) uniformly (homogeneous), 2) biased toward the low-threshold units (gradient), 3) heterogeneously with either low or high variance (heterogeneous), and 4) distributed into two groups, one receiving low inhibition and the other high inhibition. Each scenario was run 10 times and compared to a Control scenario with no inhibition. **Panel C** shows individual examples of the relationship between the change in discharge rate compared to Control and the recruitment threshold for each recruited motor unit. **Panel D** summarizes the results from the 10 simulations, with each dot representing a motor unit and each unfilled circle indicating the mean. **Panels E and F** show the two metrics used to estimate the proportion of common synaptic input, and **Panel G** shows the coefficient of determination for the relationship between the change in discharge rate relative to Control and recruitment threshold in the Control condition. On panels E, F, and G, each dot corresponds to the result of a simulation (n=10). PC1, first principal component; RT, recruitment threshold; DR, discharge rate; MVC, maximal voluntary contraction.

3. Discussion.

We investigated the behaviour of large samples of motor units during submaximal contractions under nociceptive stimulation to identify inhibitory patterns within the motor unit pool. Our experimental data, combined with *in silico* modelling, demonstrate an increase in inhibition that is non-homogeneously distributed across motor units, with evidence suggesting that this inhibition is distributed independently of motor unit size. These findings not only enhance our understanding of the wide range of motor adaptations observed during pain but also provide a framework for refining contemporary theories on how movement control is altered in response to pain.

The "pain adaptation" theory (26) proposes a decreased activation of agonist muscles to limit the amplitude or velocity of the painful movements. This theory aligns with the reduction in motor unit discharge rate observed during contractions with matched force in the presence of noxious stimulation; reviewed in (27). However, since discharge rate is a key determinant of muscle force, other changes in motor output must occur to maintain force during pain, such as an increased discharge rate in some motor units or the recruitment of additional units (10). This aligns with emerging evidence showing non-homogeneous effects of noxious stimulation across motor units (4, 6, 8, 10). Our results support these findings, showing that despite an overall significant decrease in discharge rate, a proportion of motor units did not show this decrease, and some even exhibited an increase in discharge rate (24.8% of motor units during trapezoidal contractions; Figure 1). Our aim was to gain deeper insights into the neural mechanisms underlying these variable responses within the motor unit pool.

Changes in motor unit discharge rate during pain can result from changes in the net synaptic input to motor neurons or from changes in motor neuron excitability driven by neuromodulatory inputs. Neuromodulatory drive modulates persistent inward currents in motor neuron dendrites, amplifying excitatory depolarizing currents and facilitating motor unit discharge at lower excitatory input levels than those required for recruitment, a phenomenon known as discharge rate hysteresis (14). In our study, we used a combination of approaches to assess these different effects of persistent inward currents (21). We observed a significant decrease in ΔF, an index of discharge rate hysteresis, which correlated with the decrease in discharge rate (Figure 2). However, because ΔF is largely influenced by inhibitory inputs (17, 21, 22), this change cannot be confidently attributed to a change in neuromodulatory drive. To address this limitation, we used complementary metrics that assess the deviations from a linear increase in discharge rate during the ramp-up phase of the triangular contractions (acceleration, brace height, and attenuation) (21). None of these metrics were altered during Pain, suggesting that transient experimental pain does not significantly affect the neuromodulatory drive to motor units. At first glance, this may appear inconsistent with the role of monoamines pathways in pain control (12), which could increase persistent inward currents through monoaminergic release at motor neurons. However, this mechanism has been predominantly observed in chronic pain conditions (28), and it is possible that transient pain may not be sufficient to elicit such a pain control mechanism.

As the neuromodulatory drive was not altered in the presence of pain, the overall decrease in motor unit discharge rate likely results from changes to net synaptic inputs at motor neurons. Although this could theoretically be explained by a reduction in excitatory drive, it is unlikely given that the net joint torque and muscle activation level (assessed through EMG amplitude) remained unchanged across conditions. In addition, a reduction in excitatory corticospinal drive would likely have affected all units similarly, which does not align with our results. Therefore, increased inhibitory input is most likely explanation for our experimental results. The inhibitory effects of group III and IV nociceptive afferents, which are activated by hypertonic saline, likely contribute to the reduced motor unit discharge rate during contractions with noxious stimulation (29). While this aligns with the overall decrease in discharge rate observed in our study, it does not account for the proportion of motor units that did not exhibit a decrease (Figure 1). This observation is consistent with previous reports of non-homogeneous effects of noxious stimulation within the motor unit pool. For instance, Martinez-Valdes et al. (8) observed a divergent response between low- and high-threshold units, where high-threshold units increased their discharge rate during pain, potentially compensating for the decrease in low-threshold units. As elaborated in the introduction, these results do necessarily indicate non-homogeneous inhibition across the motor unit pool, as they could result from a homogeneous inhibition that disproportionately affects low-threshold units (11). This possibility is demonstrated by our simulation results (Homogeneous inhibition, Figure 4).

To gain deeper insights into the distribution of inhibitory inputs from our large samples of motor units, we used *in silico* models to determine the inhibition schemes compatible with our experimental results. It is important to note that under the constraint of constant force output, even the Homogeneous inhibition scenario – where all the motor units received the same level of inhibitory input – could reproduce heterogeneous motor unit behaviour, with low threshold units showing decreased and higher-threshold showing increased discharge rates. However, to validate a simulation model as a plausible inhibition scheme, it needed to replicate all four key experimental observations: i) an overall decrease in discharge rate, ii) a reduced variance explained by the first principal component, iii) a reduced proportion of common input, and iv) no (or weak) relationship between the change in discharge rate and the recruitment threshold. Only two simulation scenarios met these criteria: Clustered inhibition and Heterogenous inhibition with high variance. These simulation findings strongly support a non-homogeneous distribution of inhibitory inputs to motor units, independent of their size. This may explain why newly recruited higher-threshold units during pain do not always follow the expected orderly recruitment pattern (4), a phenomenon that our simulations also revealed in the Heterogeneous or Clustered inhibition scenarios.

Although the neural basis for this non- homogeneous inhibition across the pool is not yet fully understood, several potential mechanisms can be proposed. One possibility is a differential effect of small-diameter group III and IV muscle afferents on motor neurons, with either a facilitatory or inhibitory effect, as previously suggested (30, 31). Another possibility is that motor units within the same pool receive distinct feedback, as suggested by studies on *Drosophila*, where tibia flexor motor neurons receive distinct feedback signals from leg proprioceptors (32). This pattern of non-homogeneous inhibition also aligns with theories suggesting that motor units within the same pool may receive different net inputs and thus be represented in different synergies (25). This concept is particularly well illustrated in the vastus lateralis muscle (the muscle studied here), where the activity of motor units is represented by multiple latent factors defining a multidimensional manifold (33, 34). The decreased proportion of common input reported in our experimental data suggests that the non-homogeneous distribution of group III and IV afferent feedback may shape the dimensionality of this manifold, consistent with the influence of subcortical pathways, including recurrent inhibition (34). Interestingly, a decrease in the proportion of common input has also been reported in the vastus lateralis muscle of individuals who underwent anterior cruciate ligament reconstruction (35). The purpose of such a non-homogeneous inhibition remains an open question. It may serve as a cost-effective strategy to maintain force while limiting the recruitment of additional large motor units, which have a higher metabolic cost (36). However, this hypothesis still needs to be tested.

Several methodological issues need consideration. First, nociceptive stimulation was applied to a non-muscular tissue to ensure that hypertonic saline affected only small-diameter nociceptive fibers, avoiding any impact on other axons, including motor neurons (5). However, we did not use an isotonic saline bolus injection as an additional Control condition. This is because it would have extended the protocol and increased the risk of fatigue; and based on previous reports there is no effect of isotonic saline on motor unit discharge rates (7, 8). We are confident that the observed effects were due to the painful stimulus, and not the small addition of fluid within the knee fat pad. Second, to further avoid fatigue and because ΔF validation for estimating the magnitude of persistent inward currents is not established at high force levels, our protocol was limited to contractions at 30% of MVC. Even though our results need to be confirmed across a broader range of forces, we believe that this limitation does not impact our main conclusion that a noxious stimulus induces non-homogeneous inhibition within a group of motor units with varying recruitment thresholds. Third, while EMG decomposition allowed us to identify a large sample of motor units, it cannot support conclusive outcomes regarding motor unit recruitment and de-recruitment during pain. Specifically, the inability to track a motor unit across conditions should not be directly interpreted as a change in recruitment, as it may result from the decomposition algorithm failing to identify the same motor unit between conditions. Finally, these results need to be confirmed in females as we were unable to identify enough motor units in females for estimating common input, a known limitation of surface EMG decomposition (37).

To conclude, this study provides novel insights into the distribution of inhibitory inputs to motor units during submaximal contractions performed in the presence of experimental pain. Specifically, we found that pain does not significantly alter the neuromodulatory drive to motor neurons, suggesting that the observed changes in motor unit behaviour are primarily driven by changes in inhibitory inputs. Our combined experimental and *in silico* modelling approach revealed that these inhibitory inputs are non-homogenously distributed across the motor unit pool, independent of motor unit size. These findings challenge traditional views of homogeneous inhibition during pain and provide a framework for refining contemporary theories on how movement control is affected by pain. Further work is needed to clarify the functional implications of this adaptation, particularly regarding its impact on the metabolic cost of contraction and the control of force.

4. Methods.

4.1 Participants and ethical approval

Seventeen volunteers (two females; mean±standard deviation; age: 27.0±6.5 years, height: 176.0±9.1 cm, and body mass: 73.5±14.3 kg) participated in this study. They had no history of lower leg pain that limited function, required time off work or physical activity, or necessitated consultation with a health practitioner in the six months prior to testing. The procedures were approved by the local ethics committee (The University of Queensland; 2021/HE002253). The participants were fully informed of any risks or discomfort associated with the procedures before providing written informed consent to participate. Notably, no motor units were identified in two male participants. Consequently, the results are reported for the remaining 15 participants.

4.2 Experimental design

Participants sat on a supportive chair, with their hips flexed at 80° (0° being the neutral position) and the right knee flexed at 80° (0° being the full extension). Isometric force was measured using a three-dimensional force gauge (MC3A, AMTI, USA). Inextensible straps were tightened to immobilize their torso and pelvis.

The experimental session began with a standardized warm up. After 2 min of rest, the participants performed two maximal voluntary contractions (MVC) for 3 s, with 60 s of rest in between. A third maximal contraction was performed if the difference in force between the first two contractions was greater than 10%. Peak MVC force was considered as the maximal value obtained from a moving average window of 250 ms.

The rest of the experimental session consisted of a series of isometric submaximal contractions under three different conditions: Control, during the presence of experimental pain (Pain) and after pain had ceased (Washout). For each condition, participants performed one triangular force contraction (10-s ramp up and 10-s ramp down) to 30% MVC and three trapezoidal force contractions (6-s ramp up followed by 20-s plateau at 30% MVC) interspaced by 30-s of rest. Using real-time force feedback displayed on a monitor, the participants were asked to match the target force. Because estimation of the magnitude of persistent inward currents requires that the participants accurately match the targe force, an additional triangular contraction was performed if the examiner considered that the produced force did not accurately match the triangular target force. To limit this risk, participants were first familiarized with the tasks. To minimize the impact of the preceding contractions on persistent inward currents, a two-minute rest period was systematically provided before the triangular contractions, during which the participants performed a brief knee flexion at the start of the rest.

4.3. Surface electromyographic recordings

Four adhesive grids of 64 electrodes (total of 256 electrodes) were placed over the vastus lateralis (VL) muscle (inter-electrode distance: 8 mm; GR08MM1305, OT Bioelettronica, Italy). The grids were positioned over the muscle belly to cover the largest surface while avoiding the boundaries identified by manual palpation. This setup was chosen to maximize the motor unit yield (13, 38).

Before electrode application, the skin was shaved and cleaned with an abrasive gel (Nuprep, Weaver and company, USA). The adhesive grids were held on the skin using bi-adhesive foam layers (OT Bioelettronica, Italy). Skin-electrode contact was ensured by filling the cavities of the adhesive layers with a conductive paste (AC cream, Spes Medica, Genova, Italy). A 10-cm-wide elastic band was placed over the electrodes with a slight tension to ensure that all the electrodes remained in contact with the skin throughout the experiment. A strap electrode dampened with water was placed around the contralateral ankle (ground electrode) and a reference electrode (5 × 5 cm, Kendall Medi-Trace™, Canada) was positioned over the patella of the tested limb. The EMG signals were recorded in monopolar mode, bandpass filtered (10-500 Hz) and digitized with a 16-bit precision at 2048 samples/s using a multichannel acquisition system (EMG-Quattrocento; 400-channel EMG amplifier, OT Bioelettronica, Italy).

4.4. Experimental pain.

Pain was induced by a single bolus injection of hypertonic saline (0.35 ml, 5.8% NaCl) into the infra-patellar fat pad (5) using a 25G x 16 mm needle. This injection site was chosen to avoid any direct impact of hypertonic saline on axons other than small diameter pain fibers, including the motor neurons themselves. Participants rated pain intensity throughout the Pain condition on an 11-point numerical rating scale, anchored with “no pain” at 0 and “maximum imaginable pain” at 10. After the Pain condition, participants drew the area of pain on a picture of their knee.

4.5. Data analysis

4.5.1. Amplitude of the interferential electromyographic signals

For each of the four grids, the 64 EMG signals were visually inspected for noise and artifacts. Signals identified as noisy or containing artifacts were excluded from further analysis and were replaced by the linear interpolation of all the adjacent channels (between two and four depending on the location of the electrode). Then, single differential signals were calculated as the differences between adjacent electrodes along the column direction, resulting in 59 signals per grid. These signals were rectified and averaged to provide a mean EMG amplitude value.

4.5.2. Decomposition of electromyographic signals

We used the convolutive blind source separation method (39) implemented into an open-source software [MUedit, (40)] to decompose the EMG signals into motor unit spiking activity. The automatic decomposition was performed on the monopolar EMG signals (noisy channels excluded) from one contraction per task and condition. Then, we manually edited all the motor unit spike trains following previously published procedures (41, 42). Since each trapezoidal force matching task included three contractions, we applied the edited separation vectors from the decomposed contraction to the entire signal. We then manually edited all motor units in each trapezoidal contraction. The editing process involved an iterative approach, discarding detected peaks that result in erroneous discharge rates (outliers) and adding missed discharge times that are clearly distinguishable from the noise. The motor unit pulse trains were recalculated with updated separation vectors and were accepted by the operator once all the putative discharge times were selected.

4.5.3. Motor unit tracking

EMG decomposition was performed independently on each of the four electrode grids placed over the VL muscle. As such, the same motor units could theoretically be detected across multiple grids. To identify duplicate units, we compared their spike trains. Specifically, the spike trains of each pair of motor units were initially aligned using a cross-correlation function to account for any potential delay caused by the propagation of action potentials along the fibres. Then, discharge times that occurred within 0.5 ms (1 sample) intervals were considered common between motor units, and motor units sharing more than 30% of their discharge times were considered as duplicates. In cases where duplicate units were found, only the motor unit with the lowest coefficient of variation of its inter-spike intervals was retained.

We also tracked motor units across the three conditions (Control, Pain, and Washout) for each task (trapezoidal and triangular contractions) separately. To achieve this, the separation vectors of the motor units identified in one condition was applied to the extended and whitened EMG signals of the two other conditions (19). For each of these two conditions, the resulting spike trains were compared to those initially obtained. A motor unit was considered tracked if at least 30% of the discharge times were shared. This process was applied to every potential pair of conditions. Only the motor units tracked across the three conditions were included in the analyses.

4. 5.4. Motor unit discharge characteristics

For each motor unit, the recruitment threshold was expressed as a percentage of MVC force. For the triangular contractions, recruitment time was defined as the time of the first firing. For the trapezoidal contractions, we considered the average recruitment threshold across the three contractions. We also calculated the mean discharge rate over the three torque plateaus of the trapezoidal contractions.

4.5.5. Estimates of persistent inward currents

First, we estimated the magnitude of persistent inward currents using a paired motor unit analysis applied to the triangular contractions (20). To achieve this, we smoothed the instantaneous discharge rate of each motor unit using a support vector regression (21). Then, we estimated the discharge rate of a lower-threshold motor unit (control unit) at the time of recruitment and de-recruitment of a higher-threshold motor unit (test unit). In this approach, the discharge rate of the control unit is used as a proxy for the net synaptic input to the test unit (20, 43). The difference in instantaneous discharge rate between the recruitment and de-recruitment times of the test unit, referred to as ΔF, is considered proportional to the magnitude of persistent inward currents (20). ΔF values were considered only for pairs of motor units that met the following criteria (44): (i) the test motor unit must discharge for at least 2 s, (ii) the test motor unit must be recruited at least 1 s after the control motor unit to ensure full activation of persistent inward currents, (iii) the test motor unit must be de-recruited at least 1.5 s prior to the control motor unit to prevent overestimation of ΔF, and, (iv) the smoothed discharge rate of the test and control motor units must be correlated, with a coefficient of determination (R^2) ≥ 0.7. Each reported ΔF value represents the average value across all pairs involving a given test motor unit with all possible control units (on average: 5±3 combinations; range: 1-15). As we tracked motor units across conditions, the reported ΔF values were derived from the same pairs of motor units across the three conditions (Control, Pain, and Washout).

Because ΔF values depend on both neuromodulation and inhibition supplied to the pool of motor units (17, 21), we used complementary metrics to provide a more direct estimate of the neuromodulatory inputs. Specifically, for each motor unit, we quantified the deviation from a linear increase in discharge rate relative to actual torque during the ramp-up phase of the triangular contractions (21). First, we fitted a straight line from the discharge rate at recruitment to the peak discharge rate. We calculated the brace height as the magnitude of the longest vector orthogonal to this straight line, extending to the smoothed discharge rate. To account for different recruitment threshold across motor units, and thus different ranges of discharge rates, the brace height value was normalized to the height of a right triangle whose hypotenuse represents a straight line from recruitment to peak discharge (21). We also quantified the acceleration as the slope of the linear increase between the first discharge and the instance at which the brace height occurred, and the attenuation as the slope of the linear increase between the instance at which the brace height occurred and the maximal discharge rate. Acceleration corresponds to an amplification of synaptic inputs, likely due to the activation of persistent inward currents (45).

4.5.6. Estimation of common synaptic inputs

We used two different approaches to estimate the level of dominant common synaptic inputs received by the pool of VL motor units. These analyses were conducted on the concatenated plateaus of the trapezoidal contractions, including only the motor units that fired continuously (i.e., no pause in firing longer than 250 ms).

First, we estimated the proportion of common input with respect to the total input received by the motor neuron pool (23). Specifically, we calculated the coherence between two equally sized groups of cumulative spike trains using the Neurospec toolbox (46). The number of motor units in each of the two groups varied from 1 to the maximum number (half of the total number of identified units) and 100 random permutations of the identified units were performed for each iteration. We modelled the relationship between the average coherence values in the 0-5 Hz bandwidth and the number of motor units in each group using a least-squares curve fitting approach, based on the two-parameter model described by Negro et al. (23). One parameter reflects the contribution of the common synaptic input, while the other reflects the total synaptic input. The square root of the ratio between these two parameters provides an estimate of the proportion of common synaptic input.

Second, we applied a principal component analysis to the smoothed discharge rate of motor units. All binary motor units spike trains were convoluted with a 400-ms Hanning window, such that only the oscillations of the signal related to the fluctuation of force were considered (24). These signals were high pass, bi-directionally filtered to remove offsets and trends using a Butterworth filter 2^{nd} order with a cut-off frequency of 0.75 Hz. We normalized the smoothed discharge rates between 0 and 1 to avoid any bias to the motor units with a higher greater change in discharge rate. Finally normalized smoothed discharge rates were concatenated in a n × T matrix, where n is the number of motor units and T the number of time samples. We applied principal component analysis to this matrix and quantified the variance explained by the first principal component.

4.6. In silico model

To explore potential neurophysiological mechanisms underlying the experimental results, we simulated the behaviour of motor unit pools with different distributions of inhibitory inputs, as detailed below. To this aim, we used a spiking neural network model implemented in Python [Brian 2 (47)]. The code and the list of parameters are publicly available at: https://github.com/FrancoisDernoncourt/Pain_inhibition_simulation

4.6.1. Leaky integrate and fire equations

We modelled a pool of 300 motor units using a conductance-based leaky integrate-and-fire model. Each motor neuron had a resting membrane potential and reset voltage E_{rest} of 0 mV and a firing threshold V_{thresh} of 10 mV. The change in voltage per timestep $\frac{dv}{dt}$ was calculated as a function of the leak current I_{leak} (in nA), excitatory current I_{excit} (in nA), inhibitory current I_{inhib} (in nA), and the membrane capacitance C (in F), as follows:

$$\frac{dv}{dt} = \frac{-(I_{leak} + I_{excit} + I_{inhib})}{C}$$

The current values were calculated according to the specific conductance values (g) and equilibrium potential (E), as follows:

$$I_{leak} = g_{leak} \times (v - E_{rest})$$

$$I_{excit} = \max(g_{excit} \times (v - E_{excit}) + I_{rheobase}\ , 0)$$

$$I_{inhib} = g_{inhib} \times (v - E_{inhib})$$

An offset $I_{rheobase}$ was applied to the excitatory current, which corresponds to the minimum current necessary for the excitatory conductance to be non-zero. E_{excit} was set to 25 mV, and

E_{inhib} to -15 mV. These values were chosen so that excitatory and inhibitory inputs induced a voltage change of the same magnitude when the membrane potential was halfway between E_{rest} and V_{thresh}.

The conductance values (in mS) were defined as:

$$g_{leak} = \frac{1}{R_i}$$

$$g_{excit} = \gamma_{excit}(t,i) \times S_i$$

$$g_{inhib} = \gamma_{inhib}(t,i) \times S_i$$

where R_i (in Ohms) represents the membrane resistance of a given motor neuron i, $\gamma_{excit}(t,i)$ and $\gamma_{inhib}(t,i)$ are the time-dependent excitatory and inhibitory synaptic inputs delivered to each motor neuron i at each timestep t, and S_i is a scaling factor representing the responsiveness of the membrane potential to a given input. S_i values were calculated as the normalized resistance of motor neurons, with S_i of the smallest motor neuron set to 1. After firing, motor neurons underwent a refractory period $T_{refractory}$ during which the membrane potential was clamped to 0 mV.

4.6.2. Motor unit properties

Each motor neuron i within the pool was assigned a specific soma diameter D_i (in µm), which was assigned according to the following quadratic function, ranging from 50 µm (D_{min}) to 100 µm (D_{max}):

$$D_i = D_{min} + (\frac{i}{N})^2 \times (D_{max} - D_{min})$$

This distribution ensured a higher representation of low-threshold motor neurons (48). The relationship between the soma diameter and R, C, $I_{rheobase}$ and $T_{refractory}$ was determined using the equations provided by Caillet et al. (49) (for additional details, please see the code).

To simulate the torque profiles generated by the active motor units, each unit was associated to specific twitch properties, with the torque of a single twitch ranging from 5 mN.m (smallest unit) to 140 mN.m (largest unit) and a time-to-peak ranging from 20 ms (largest unit) to 80 ms (smallest unit) (50). Both twitch torque and time-to-peak values were determined from linear interpolation based on the normalized soma diameter. Note that the ratio between a single twitch torque and tetanus torque ranged from 0.2 (smallest motor unit) to 0.3 (largest motor unit) (51). The total torque output of the motor unit pool was obtained by summing the absolute torque profiles of all active units. A low-pass filter (5th order Butterworth, bi-directional, cut-off: 10 Hz) was applied to the total force output to account for the mechanical impedance of the muscle-tendon unit.

2.6.3. Input to the simulated neurons

The simulated motor units received common excitatory input, common noise (0-5 Hz bandwidth) and independent noise (0-50 Hz bandwidth). The independent and common noise were modelled as low-pass-filtered Gaussian noise with a mean of 0 mS and a standard deviation (SD) of 0.03 and 0.015 mS, respectively. All the motor units within the pool received the same common excitatory input and common noise, while each motor unit received different independent noise. We estimated the common excitatory input signal required for the pool of motor units to match a target force plateau at 30% of MVC, i.e. about 12 N.m for the number of simulated motor units. This process involved an optimization procedure with the Adam optimizer (52).

We tested the six simulation scenarios described in the *Results* section.The mean level of inhibition was maintained constant across the five scenarios with inhibition, and the force was kept constant. To achieve this, the optimization procedure to determine the excitatory input (as described above) was performed after applying inhibition. Also, to account for the biased excitatory inputs toward larger motor neurons (53), the weight of the excitatory inputs was slightly adjusted, with lower values assigned to smaller motor units and higher values to larger ones, and linearly interpolated between them.

While only one simulation was run for the Control condition, ten simulations were run for the conditions with inhibition to account for slightly different distribution on inhibitory inputs across the simulations. Simulations were conducted over a 60-s period, corresponding to the three 20-s plateaus in the experimental setup. We pre-processed and analysed the simulated spike trains of the active motor units using the same methods as for the experimentally recorded spike trains (see above). Of note, only the motor units that fired continuously were included in the analysis.

4.7. Statistics

All statistical analyses were performed with RStudio (USA). First, the normality of the data distribution was assessed using quantile-quantile plots and histograms. Separate linear mixed-effects models, implemented in the *lmerTest* package, were applied to compare the outcomes across conditions. In these models, ‘condition’ (Control, Pain, Washout) was treated as a fixed effect, and ‘participants’ were modeled as random intercepts. When necessary, multiple comparisons were performed using the *emmeans* package, using the Tukey method to adjust the *p*-values.

We ran Pearson correlations to examine the relationship between the change in motor unit discharge rate across conditions and either the ΔF value or the recruitment threshold from the Control condition. The significance level was set at $p<0.05$, and all values are reported as mean ± SD.

5. References.

1. C. S. Sherrington, *The integrative action of the nervous system* (New Haven, CTYale University, 1906).
2. D. Farina, L. Arendt-Nielsen, T. Graven-Nielsen, Experimental muscle pain reduces initial motor unit discharge rates during sustained submaximal contractions. *J Appl Physiol (1985)* **98**, 999-1005 (2005).
3. M. K. Sohn, T. Graven-Nielsen, L. Arendt-Nielsen, P. Svensson, Inhibition of motor unit firing during experimental muscle pain in humans. *Muscle Nerve* **23**, 1219-1226 (2000).
4. K. Tucker, J. Butler, T. Graven-Nielsen, S. Riek, P. Hodges, Motor unit recruitment strategies are altered during deep-tissue pain. *J Neurosci* **29**, 10820-10826 (2009).
5. K. J. Tucker, P. W. Hodges, Motoneurone recruitment is altered with pain induced in non-muscular tissue. *Pain* **141**, 151-155 (2009).
6. F. Hug, P. W. Hodges, K. J. Tucker, Effect of pain location on spatial reorganisation of muscle activity. *J Electromyogr Kinesiol* **23**, 1413-1420 (2013).
7. E. Martinez-Valdes, F. Negro, M. Arvanitidis, D. Farina, D. Falla, Pain-induced changes in motor unit discharge depend on recruitment threshold and contraction speed. *J Appl Physiol (1985)* **131**, 1260-1271 (2021).
8. E. Martinez-Valdes, F. Negro, D. Farina, D. Falla, Divergent response of low- versus high-threshold motor units to experimental muscle pain. *J Physiol* **598**, 2093-2108 (2020).
9. H. R. Luscher, P. Ruenzel, E. Henneman, How the size of motoneurones determines their susceptibility to discharge. *Nature* **282**, 859-861 (1979).
10. P. W. Hodges, K. Tucker, Moving differently in pain: a new theory to explain the adaptation to pain. *Pain* **152**, S90-S98 (2011).
11. R. N. O. Mesquita, J. Skarabot, G. E. P. Pearcey, Low-threshold motor units can be a pain during experimental muscle pain. *J Physiol* **598**, 2545-2547 (2020).
12. I. Martins, I. Tavares, Reticular Formation and Pain: The Past and the Future. *Front Neuroanat* **11**, 51 (2017).
13. S. Avrillon, F. Hug, R. Enoka, A. Caillet, A. Farina, The decoding of extensive samples of motor units in human muscles reveals the rate coding of entire motoneuron pools. *BioRxiv* https://doi.org/10.1101/2023.11.25.568607 (2023).
14. R. H. Lee, C. J. Heckman, Bistability in spinal motoneurons in vivo: systematic variations in rhythmic firing patterns. *J Neurophysiol* **80**, 572-582 (1998).
15. H. Hultborn, M. E. Denton, J. Wienecke, J. B. Nielsen, Variable amplification of synaptic input to cat spinal motoneurones by dendritic persistent inward current. *J Physiol* **552**, 945-952 (2003).
16. A. S. Hyngstrom, M. D. Johnson, J. F. Miller, C. J. Heckman, Intrinsic electrical properties of spinal motoneurons vary with joint angle. *Nat Neurosci* **10**, 363-369 (2007).
17. A. L. Revill, A. J. Fuglevand, Inhibition linearizes firing rate responses in human motor units: implications for the role of persistent inward currents. *J Physiol* **595**, 179-191 (2017).
18. P. W. Hodges *et al.*, Non-uniform Effects of Nociceptive Stimulation to Motoneurones during Experimental Muscle Pain. *Neuroscience* **463**, 45-56 (2021).
19. A. Francic, A. Holobar, On the Reuse of Motor Unit Filters in High Density Surface Electromyograms Recorded at Different Contraction Levels. *IEEE Access* **9**, 115227-115236 (2021).
20. M. Gorassini, J. F. Yang, M. Siu, D. J. Bennett, Intrinsic activation of human motoneurons: possible contribution to motor unit excitation. *J Neurophysiol* **87**, 1850-1858 (2002).
21. J. A. Beauchamp *et al.*, A geometric approach to quantifying the neuromodulatory effects of persistent inward currents on individual motor unit discharge patterns. *J Neural Eng* **20** (2023).
22. M. K. Chardon *et al.*, 10.1101/2022.12.09.519818 (2023).

23. F. Negro, U. S. Yavuz, D. Farina, The human motor neuron pools receive a dominant slow-varying common synaptic input. *J Physiol* **594**, 5491-5505 (2016).
24. F. Negro, A. Holobar, D. Farina, Fluctuations in isometric muscle force can be described by one linear projection of low-frequency components of motor unit discharge rates. *J Physiol* **587**, 5925-5938 (2009).
25. F. Hug, S. Avrillon, J. Ibanez, D. Farina, Common synaptic input, synergies and size principle: Control of spinal motor neurons for movement generation. *J Physiol* **601**, 11-20 (2023).
26. J. P. Lund, R. Donga, C. G. Widmer, C. S. Stohler, The pain-adaptation model: a discussion of the relationship between chronic musculoskeletal pain and motor activity. *Can J Physiol Pharmacol* **69**, 683-694 (1991).
27. A. Sanderson *et al.*, The effect of experimental and clinical musculoskeletal pain on spinal and supraspinal projections to motoneurons and motor unit properties in humans: A systematic review. *Eur J Pain* **25**, 1668-1701 (2021).
28. K. Bannister, L. A. Bee, A. H. Dickenson, Preclinical and early clinical investigations related to monoaminergic pain modulation. *Neurotherapeutics* **6**, 703-712 (2009).
29. S. Mense, Nociception from skeletal muscle in relation to clinical muscle pain. *Pain* **54**, 241-289 (1993).
30. K. D. Kniffki, E. D. Schomburg, H. Steffens, Synaptic effects from chemically activated fine muscle afferents upon α-motoneurones in decerebrate and spinal cats. *Brain Research* **206**, 361-370 (1981).
31. P. G. Martin, J. L. Smith, J. E. Butler, S. C. Gandevia, J. L. Taylor, Fatigue-sensitive afferents inhibit extensor but not flexor motoneurons in humans. *J Neurosci* **26**, 4796-4802 (2006).
32. A. W. Azevedo *et al.*, A size principle for recruitment of Drosophila leg motor neurons. *Elife* **9** (2020).
33. A. Del Vecchio *et al.*, The Forces Generated by Agonist Muscles during Isometric Contractions Arise from Motor Unit Synergies. *J Neurosci* **43**, 2860-2873 (2023).
34. F. Dernoncourt *et al.*, Flexible Control of Motor Units: Is the Multidimensionality of Motor Unit Manifolds a Sufficient Condition? *BioRxiv* https://doi.org/10.1101/2024.07.23.604408 (2024).
35. S. Nuccio *et al.*, Neuroplastic alterations in common synaptic inputs and synergistic motor unit clusters controlling the vastii muscles of individuals with ACL reconstruction. *J Appl Physiol (1985)* **137**, 835-847 (2024).
36. J. R. Zierath, J. A. Hawley, Skeletal muscle fiber type: influence on contractile and metabolic properties. *PLoS Biol* **2**, e348 (2004).
37. C. A. Taylor, B. H. Kopicko, F. Negro, C. K. Thompson, Sex differences in the detection of motor unit action potentials identified using high-density surface electromyography. *J Electromyogr Kinesiol* **65**, 102675 (2022).
38. A. H. Caillet *et al.*, Larger and Denser: An Optimal Design for Surface Grids of EMG Electrodes to Identify Greater and More Representative Samples of Motor Units. *eNeuro* **10** (2023).
39. F. Negro, S. Muceli, A. M. Castronovo, A. Holobar, D. Farina, Multi-channel intramuscular and surface EMG decomposition by convolutive blind source separation. *J Neural Eng* **13**, 026027 (2016).
40. S. Avrillon, F. Hug, S. N. Baker, C. Gibbs, D. Farina, Tutorial on MUedit: An open-source software for identifying and analysing the discharge timing of motor units from electromyographic signals. *J Electromyogr Kinesiol* **77**, 102886 (2024).
41. A. Del Vecchio *et al.*, Tutorial: Analysis of motor unit discharge characteristics from high-density surface EMG signals. *J Electromyogr Kinesiol* **53**, 102426 (2020).
42. F. Hug *et al.*, Analysis of motor unit spike trains estimated from high-density surface electromyography is highly reliable across operators. *J Electromyogr Kinesiol* **58**, 102548 (2021).
43. M. A. Gorassini, D. J. Bennett, J. F. Yang, Self-sustained firing of human motor units. *Neurosci Lett* **247**, 13-16 (1998).

44. A. Hassan *et al.*, Impact of parameter selection on estimates of motoneuron excitability using paired motor unit analysis. *J Neural Eng* **17**, 016063 (2020).
45. R. H. Lee, C. J. Heckman, Adjustable amplification of synaptic input in the dendrites of spinal motoneurons in vivo. *J Neurosci* **20**, 6734-6740 (2000).
46. D. M. Halliday, Nonparametric directionality measures for time series and point process data. *J Integr Neurosci* **14**, 253-277 (2015).
47. M. Stimberg, R. Brette, D. F. Goodman, Brian 2, an intuitive and efficient neural simulator. *Elife* **8** (2019).
48. J. Duchateau, R. M. Enoka, Distribution of motor unit properties across human muscles. *J Appl Physiol (1985)* **132**, 1-13 (2022).
49. A. H. Caillet, A. T. M. Phillips, D. Farina, L. Modenese, Mathematical relationships between spinal motoneuron properties. *Elife* **11** (2022).
50. M. Van Cutsem, P. Feiereisen, J. Duchateau, K. Hainaut, Mechanical properties and behaviour of motor units in the tibialis anterior during voluntary contractions. *Can J Appl Physiol* **22**, 585-597 (1997).
51. I. E. Brown, G. E. Loeb, Measured and modeled properties of mammalian skeletal muscle: IV. dynamics of activation and deactivation. *J Muscle Res Cell Motil* **21**, 33-47 (2000).
52. D. P. Kingma, J. Ba, Adam: A Method for Stochastic Optimization. *arXiv* https://doi.org/10.48550/arXiv.1412.6980 (2014).
53. C. J. Heckman, R. M. Enoka, Motor unit. *Compr Physiol* **2**, 2629-2682 (2012).

A. Trapezoidal contractions

Control
Pain
Wash out
Mean discharge rate (pps)
15
12.5
10
7.5
5
Change in discharge rate (pps)
1
0
−1
−2
−3
1
2
3
4
5
6
7
10
11
12
13
14
15
16
17
Participant #
Change in discharge rate (pps)
1
0
−1
−2
−3
0
10
20
30
Recruitment threshold (% MVC)

B. Triangular contractions

Max discharge rate (pps)
20
15
10
5
Change in discharge rate (pps)
2
0
−2
−4
1
2
3
4
5
6
7
10
11
12
13
14
15
16
17
Participant #
Change in discharge rate (pps)
1
0
−1
−2
−3
−4
6
9
12
15
Recruitment threshold (% MVC)

A.
Control
Pain
Wash out
ΔF (pps)
5
5
2.5
0
−2.5
Change in ΔF (pps)
3
2
1
0
−1
−2
Participant #
1
3
4
5
6
10
11
13
14
15
16
17
B.
Change in discharge rate
(Pain − Control, in pps)
1
0
−1
−2
−3
−4
Change in ΔF
(Pain − Control, in pps)
−2
−1
0
1
2
3
C.
Attenuation
Acceleration
Brace
height
Instantaneous
discharge rate
time
Brace height
%
80
60
40
20
0
Control
Pain
Wash out
Acceleration
pps / %MVC
2.5
2
1.5
1
0.5
0
Control
Pain
Wash out
Attenuation
pps / %MVC
1
0.75
5
0.25
0
Control
Pain
Wash out

A.
Proportion of common input
0.5
0.4
0.3
0.2
0.1
*
*
Control
Pain
Wash out
B.
% variance explained by PC1
60
40
20
*
*
Control
Pain
Wash out

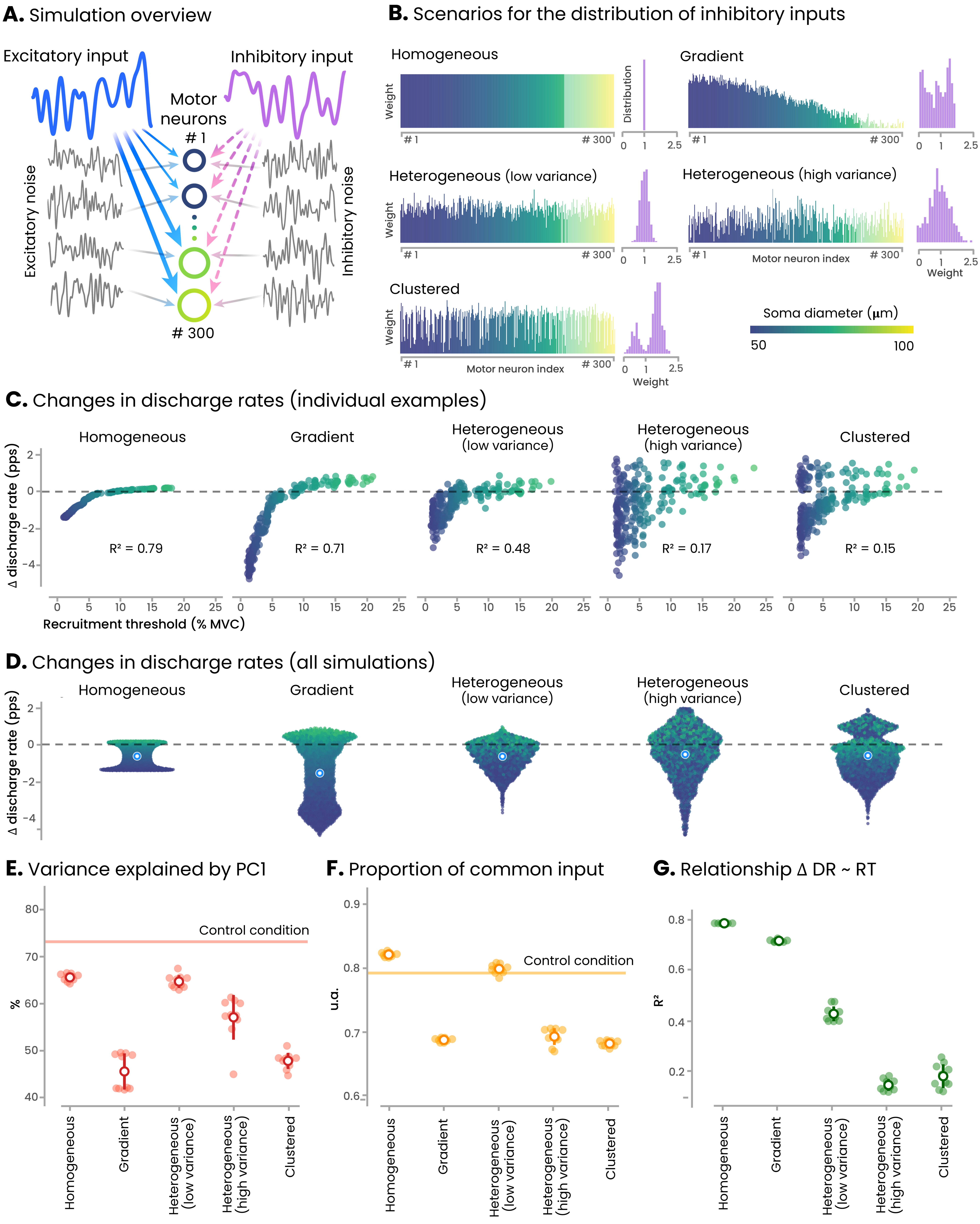

A. Simulation overview
Excitatory input
Inhibitory input
Motor neurons
# 1
# 300
Excitatory noise
Inhibitory noise
B. Scenarios for the distribution of inhibitory inputs
Homogeneous
Gradient
Heterogeneous (low variance)
Heterogeneous (high variance)
Clustered
Weight
Distribution
# 1
# 300
0
1
2.5
Motor neuron index
Weight
Soma diameter (μm)
50
100
C. Changes in discharge rates (individual examples)
Homogeneous
Gradient
Heterogeneous (low variance)
Heterogeneous (high variance)
Clustered
Δ discharge rate (pps)
2
0
-2
-4
R² = 0.79
R² = 0.71
R² = 0.48
R² = 0.17
R² = 0.15
0
5
10
15
20
25
Recruitment threshold (% MVC)
D. Changes in discharge rates (all simulations)
Homogeneous
Gradient
Heterogeneous (low variance)
Heterogeneous (high variance)
Clustered
Δ discharge rate (pps)
2
0
-2
-4
E. Variance explained by PC1
%
80
70
60
50
40
Control condition
F. Proportion of common input
u.a.
0.9
0.8
0.7
0.6
Control condition
G. Relationship Δ DR ~ RT
R²
0.8
0.6
0.4
0.2
Homogeneous
Gradient
Heterogeneous (low variance)
Heterogeneous (high variance)
Clustered